Brain Stimulation 14 (2021) 1154–1168

Contents lists available at ScienceDirect

Brain Stimulation

journal homepage: http://www.journals.elsevier.com/brain-stimulation

Adaptive current-flow models of ECT: Explaining individual static impedance, dynamic impedance, and brain current density

Gozde Unal [a, *], Jaiti K. Swami [a], Carliza Canela [a], Samantha L. Cohen [b], Niranjan Khadka [c], Mohamad FallahRad [a], Baron Short [d], Miklos Argyelan [e], Harold A. Sackeim [f], Marom Bikson [a]

[a] Department of Biomedical Engineering, The City College of New York, CUNY, New York, NY, USA
[b] Department of Biomedical Engineering, Cornell University, Ithaca, NY, 14850, USA
[c] Department of Psychiatry, Laboratory for Neuropsychiatry and Neuromodulation, Massachusetts General Hospital, Harvard Medical School, MA, USA
[d] Department of Psychiatry and Behavioral Sciences, Medical University of South Carolina, Charleston, SC, USA
[e] Center for Neurosciences, The Feinstein Institute for Medical Research, North Shore- Long Island Jewish Health System, Manhasset, NY, 11030, USA
[f] Department of Psychiatry and Radiology, Vagelos College of Physicians and Surgeons, Columbia University, New York, USA

ARTICLE INFO

Article history:
Received 13 December 2020
Received in revised form
19 July 2021
Accepted 22 July 2021
Available online 28 July 2021

ABSTRACT

Background: Improvements in electroconvulsive therapy (ECT) outcomes have followed refinement in device electrical output and electrode montage. The physical properties of the ECT stimulus, together with those of the patient's head, determine the impedances measured by the device and govern current delivery to the brain and ECT outcomes.

Objective: However, the precise relations among physical properties of the stimulus, patient head anatomy, and patient-specific impedance to the passage of current are long-standing questions in ECT research and practice. To this end, we develop a computational framework based on diverse clinical data sets.

Methods: We developed anatomical MRI-derived models of transcranial electrical stimulation (tES) that included changes in tissue conductivity due to local electrical current flow. These "adaptive" models simulate ECT both during therapeutic stimulation using high current (~1 A) and when dynamic impedance is measured, as well as prior to stimulation when low current (~1 mA) is used to measure static impedance. We modeled two scalp layers: a superficial scalp layer with adaptive conductivity that increases with electric field up to a subject-specific maximum ($\sigma_{\overline{SS}}$), and a deep scalp layer with a subject-specific fixed conductivity (σ_{DS}).

Results: We demonstrated that variation in these scalp parameters may explain clinical data on subject-specific static impedance and dynamic impedance, their imperfect correlation across subjects, their relationships to seizure threshold, and the role of head anatomy. Adaptive tES models demonstrated that current flow changes local tissue conductivity which in turn shapes current delivery to the brain in a manner not accounted for in fixed tissue conductivity models.

Conclusions: Our predictions that variation in individual skin properties, rather than other aspects of anatomy, largely govern the relationship between static impedance, dynamic impedance, and ECT current delivery to the brain, themselves depend on assumptions about tissue properties. Broadly, our novel modeling pipeline opens the door to explore how adaptive-scalp conductivity may impact transcutaneous electrical stimulation (tES).

1. Introduction

Ongoing advancements in the efficacy or specificity (reduced adverse effects) of electroconvulsive therapy (ECT) rely on refinement in dose; namely electrode montage and stimulation

* Corresponding author.
E-mail addresses: gunal000@citymail.cuny.edu (G. Unal), bikson@ccny.cuny.edu (M. Bikson).

https://doi.org/10.1016/j.brs.2021.07.012

waveform, and intensity [1,2]. Dose optimization has followed heuristic approaches, and controversies remain unreconciled despite decades of research [3,4]. Modern ECT devices deliver current-controlled (800–900 mA) pulses, so that applied voltage is adjusted based on the encountered impedance. Devices report the resulting "dynamic impedance" during the passage of the ECT stimulus. Prior to stimulation, ECT devices report a "static impedance" using low intensity (~1 mA) high-frequency test currents. While static impedance and dynamic impedance has long been recognized as markers of individual differences, their etiology and consequences are undetermined [5] – including how they impact on seizure induction [6–9].

The finding that dynamic impedance is lower than static impedance is consistent with an increase in tissue conductivity in response to high (dynamic impedance) verse low (static impedance) current intensity. But it is unclear which tissue layers are responsible for this impedance difference, how current flow to the brain is then altered, and with what implications to seizure genesis?

While significant covariation between static and dynamic impedance has been reported [10], debate about whether there is a meaningful correlation has spanned decades [5,11,12]. One aim of this study was to explain the imperfect relationship between static and dynamic impedance. We use clinical trial datasets with standardized electrode preparation conditions to reexamine the relations between static and dynamic impedance values under fastidious conditions. In a sample of normal subjects, we systematically manipulated electrode preparation factors (contact area, adherence) to determine the impact of preparation protocol on static impedance across subjects. Novel current-flow models were developed and experientially constrained based on ECT subjects anatomical imaging and impedance data, to systematically explain what factors drive versus limit the correlation between static and dynamic impedance.

For a given ECT electrical dose, the pattern of current delivery to the brain is determined by individual anatomy and electric conductivity of each tissue compartment (e.g. skin, skull) [10,13,14]. In theory, changing tissue conductivity during the passage of the ECT stimulus would influence the distribution of current density in brain. Correlations between dynamic impedance and seizure threshold have been shown [10] but not reliably [8,9]. A further aim of this study, using current-flow models, is to understand how changing tissue conductivity (alongside other anatomical factors) govern brain current flow during ECT and how this is reflected in overall impedance.

We developed an individualized (MRI-derived) finite element method (FEM) to model transcranial electrical stimulation while incorporating "adaptive" changes in tissue conductivity by local current flow. These models explain the source of individual difference in ECT static and dynamic impedance, how they relate, and how they impact seizure threshold. More generally, these state-of-the-art models demonstrate that adaptive change in tissue conductivity shapes current delivery across the head, resulting in different patterns than predicted by fixed-conductivity models.

2. Methods

2.1. Electrode preparation on static impedance: controlled experiments in healthy subjects

We conducted a study to evaluate the role of electrode preparation on static impedance using healthy subjects (n = 3) within whom six electrode preparation techniques could be compared. The study was conducted in accordance to the protocols and procedures approved by the Institutional Review Board of the City University of New York. All comparisons were made using disposable, adherent pads as electrodes (Thymapads, Somatics, LLC, Venice, Fl). The electrode preparation techniques included: 1) Skin cleaning with saline and application of Pretac (Pharmaceutical Innovations, Newark, New Jersey); 2) Skin cleaning with alcohol (99 %) and application of Pretac; 3) Skin cleaning with saline and application of Pretac but with only 50 % electrode contact area (achieved with using a plastic insulative sheet with a 2.5 × 2.5 cm annulus); 4) Skin cleaning with alcohol only; 5) Skin cleaning with saline and application of polyvinylpyrrolidone (PVP–K90, 1 % w/v) (Sigma-Aldrich Inch, St. Louis, Missouri); 6) Skin cleaning with saline and application of PVP-K90 plus potassium chloride (KCL, 0.0003 %). Pretac or PVP-K90 was applied to the disposable electrode surfaces (300–500 μL) before placement on the skin. Electrodes were positioned according to the standard bifrontal placement [15], avoiding hairline, with careful attention to ensure uniform electrode-skin contact. Static impedance was measured using both a SpECTrum 5000Q (MECTA Corporation, Tualatin, OR) and Thymatron System IV (Somatics LLC) ECT device, immediately after electrode application (t = 0) and every minute for 17 min or until a stable impedance was recorded. Each subject and electrode preparation combination was tested 3 times, with tests separated by > 1 day.

2.2. RUL and BL clinical ECT data set, New York state Psychiatric Institute

Anonymized data was re-analyzed from a New York State Psychiatric Institute ECT trial [16] using right unilateral (RUL) and bilateral (BL) ECT. For this series, only stimulation at 800 mA was included in our analysis. Ninety patients in an episode of major depression were randomized into four groups in a 2 × 2 design, varying both electrode placement and pulse duration (0.3 ms vs. 1.5 ms). Except for the pulse width manipulation, stimulation waveform was identical in the ultra-brief and brief pulse groups. 5 cm stainless steel circular disk electrodes were used with handheld electrode assemblies (MECTA Corporation). Seizure threshold was quantified at the first and last treatments using a titration procedure. At all other treatment sessions electrical dosage was 2.5 or 6.0 times the seizure threshold quantified at the first titration session for BL ECT and RUL ECT, respectively. While precision of seizure threshold may be limited by resolution of titration steps and "floor effects," [8] it is relatively established that this approach shows increasing seizure threshold with decreasing dynamic impedance [8,9] for RUL and BL montages.

2.3. BF clinical ECT data set, North Shore- Long Island Jewish Health System

Anonymized data was analyzed from a North Shore- Long Island Jewish Health System ECT trial series [17] using bifrontal (BF) ECT. 4.2 × 4.9 cm disposable adhesive electrodes were used (Thymapads, Somatics LLC). Each subject received 6–10 ECT sessions with electrodes configured in a bifrontal montage (with Pretac preparation). High resolution T1-weighted anatomical MRIs were deidentified from a cohort of subjects (n = 17) receiving ECT (see modeling below). MR imaging exams were conducted at North Shore University Hospital on a 3 T GE HDx scanner (General Electric, Milwaukee, WI, USA). We acquired structural scans in the coronal plane using a three-dimensional spoiled gradient sequence (TR = 7.5 ms, TE = 3 ms, matrix = 256 × 256, FOV = 240 mm), producing 216 contiguous images (slice thickness = 1 mm) through the whole head.

2.4. BF/RUL clinical ECT data set, Medical University of South Carolina

Anonymized data was analyzed from a Medical University of South Carolina ECT trial series using BF and RUL ECT with varying pulse duration (0.3 ms vs 0.5 ms). The study was conducted in accordance to the protocols and procedures approved by the Institutional Review Board of the Medical University of South Carolina. For this series, both 600 and 900 mA was applied to each patients (n = 10). 5 cm stainless steel circular disk electrodes were used with hand-held electrode assemblies (MECTA Corporation).

2.5. General computational modeling approach

Skin impedance decreases with increasing electrical current density, to a skin-specific asymptote of ~0.1–0.5 S/m at ~500 μA/cm^2 [18–20]. However, ECT average electrode current density (current divided by electrode area) is > 30 mA/cm^2. Overall head impedance decreases with increasing ECT current density, to a subject-specific asymptote of ~200 Ohm at <800 mA and <200 V [5,11]. At low current, minimum skin resistivity varies substantially with tested-conditions and across microscopic layers, spanning ~1*10^{-5} S/m for epidermal stratum corneum and ~2*10^{-4} to 0.2 S/m for layers of dermis and fat [21,22]. This range can be contrasted with a skull conductivity of ~0.01 S/m.

It is intractable to model <0.1 mm thick tissue layers at full head-scale, necessitating approximation [23]. Adjacent tissue layers with mismatched resistivity can especially impact on current flow patterns [24,25]. Given the above, we consider two scalp layers: a "superficial-scalp" layer and "deep-scalp" layer in the models. The deep-scalp layer is considered to have low conductivity, that is fixed (not effected by current flow). The superficial scalp has minimal conductivity at low current (conditions of static impedance) and high conductivity at high current (conditions of dynamic impedance).

The capacitive effects in biological tissues can be generally neglected when modeling electrical stimulation [26] and are negligible when measured during ECT [10]. Lumped-parameter model of skin use capacitors in parallel with non-linear (current dependent) resistances [18,19]. Capacitive properties of tissue, notably skin layers, decrease at either high current [27] or at high frequency. Indeed, the notion that low-intensity (sub-perception) high-frequency (>7 kHz) current can be used during preparation to estimate subject resistance during passage of the ECT stimulus dates to at least 1942 [28], and is reflected in contemporary use of high-frequency to test static impedance. Therefore, we do not model tissue permittivity. We represent the non-linear changes in resistivity to current flow. The validity of the quasi-static approximation was directly verified for the case of a point source electrode in an infinite, homogeneous, isotropic volume [29], without electric field magnitude dependent tissue-properties. Consistent with our objective, their analysis affirmed that stimulation predictions are most sensitive to the representation of tissue conductivity.

2.6. Subject head segmentation, subject-generic tissue parameterization, and electrodes

Of the seventeen subjects in North Shore- Long Island Jewish Health System ECT series cohort, high resolution MRI-derived head models were developed for four subjects (#21908, #22615, #22035, #21778), selected based on a range and variance in static and dynamic impedance values. An automated segmentation pipeline based on algorithms in SPM8 [30] and updated for volume conduction models [31] was used to create initial image masks of scalp, skull, air, meninges/cerebrospinal fluid, gray matter and white matter (Fig. 1 B). Additional manual segmentation was applied to correct for noise, aliasing artifacts, and to separate superficial scalp and deep scalp layers (approximately bisecting the scalp mask).

Unless otherwise indicated, these segmented tissues were assigned subject-independent and fixed (not electric field dependent) electrical conductivity [23]: skull (σ = 0.01 S/m), gray matter (σ = 0.276 S/m), white matter (σ = 0.126 S/m), meninges/cerebrospinal fluid (σ = 0.85 S/m), and air (σ = 1*10^{-15} S/m). Deep-scalp layer was assigned a subject-specific but fixed (not electric field dependent) conductivity (σ_{DS}) between 4.5*10^{-4} S/m and 0.008 S/m. Local superficial-scalp layer conductivity (σ_{SS}) was a function of local scalp electric field (E_{SS}) given by:

$$\sigma_{SS} = \begin{cases} A, & 0 < E_{SS} < B \\ C*E_{SS} - D, & B \le E_{SS} < E_{\overline{SS}} \\ \sigma_{\overline{SS}}, & E_{SS} \ge E_{\overline{SS}} \end{cases} \quad (1)$$

Where $\sigma_{\overline{SS}}$ is subject-specific maximum superficial-scalp conductivity. We emphasize that E_{SS} varies across the scalp surface such that σ_{SS} then varies across the head (higher near electrodes). Across subjects, four parameters (A, B, C, D) were fixed (Table 1). For each subject two model parameters were individualized: deep-scalp layer conductivity (σ_{DS}) and maximum superficial-layer conductivity $\sigma_{\overline{SS}}$. In addition, $E_{\overline{SS}}$ is subject specific and determined by Equation (1).

To summarize, the calculation of current flow model is based on five assumptions:

1. Scalp is divided into two layers.
2. Deep-scalp layer conductivity is subject-specific, isotropic, and fixed.
3. Local superficial-scalp layer conductivity increases instantly and linearly with local E_{SS}, starting at a threshold, to a subject-specific maximum ($E_{\overline{SS}}$).
4. Other tissues (skull, meninges/cerebrospinal fluid, gray/white matter, air) have subject-independent, fixed, isotropic conductivities.
5. Capacitive effects/tissue permittivity are assumed negligible.

Ultimately, this is a novel heuristic approach that is computational tractable, supporting data interpretation and device design (see Discussion). This approach borrows from lumped-parameter skin impedance models that consider a current-sensitive superficial layer and a current-insensitive deep layer with relatively low conductivity [18–20]. A previous model simulating ECT during pregnancy [32] implemented a single skin layer with (un-saturated) conductivity changes restricted under the electrodes.

We modeled two electrode configurations, with electrode shape and position corresponding to the clinical series studied:

1. Bifrontal (BF) pad electrode montage: The centers of both electrodes are on a first imaginary line that originates at the lateral canthus and projects up parallel to the facial midline. The long edge of the electrodes is aligned parallel to the first imaginary line such that the short edge of the pad electrodes is approximately parallel to the horizontal plane. The short edge of the pad electrodes is right above supraorbital ridge (approximately above the eyebrow). Depending on the subject, the

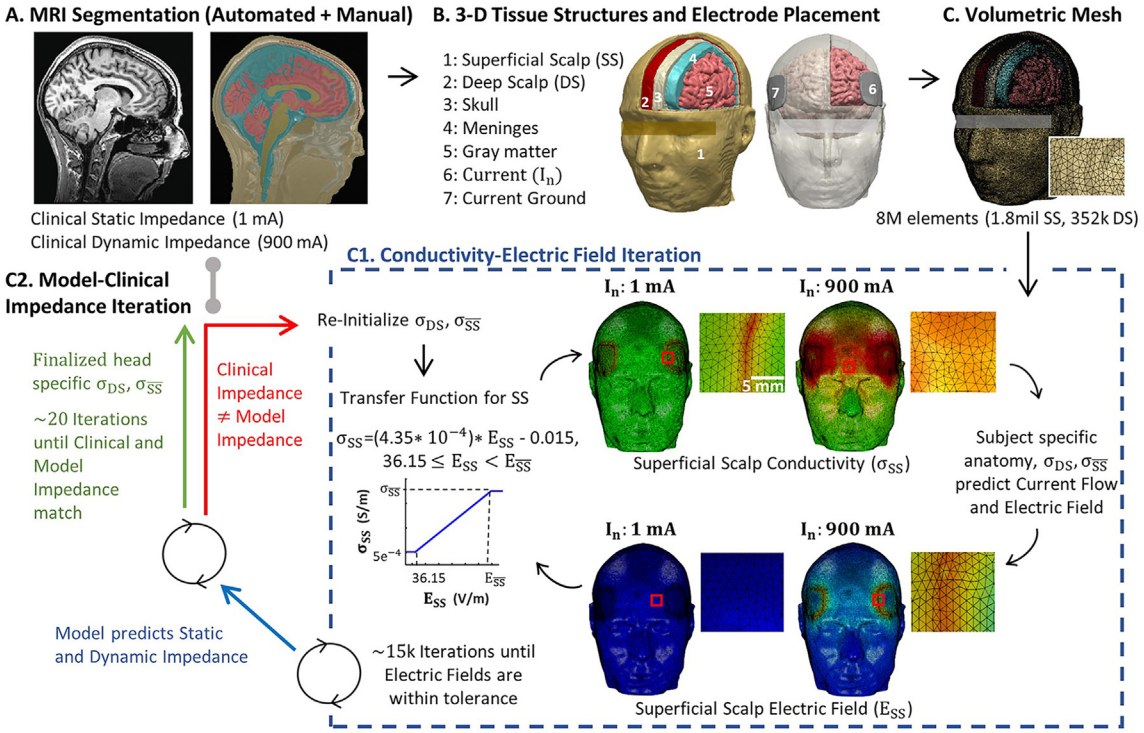

Fig. 1. Novel adaptive computational pipeline for ECT current flow FEM models. We developed the first image-derived numerical models of transcranial electrical stimulation (tES) incorporating local changes in tissue conductivity in response to local current flow (electric fields). (A) T1-weighted anatomical MRIs were collected from ECT patients, with static impedance and dynamic impedance data. (B) Volume conductor models were created preserving image resolution using methods previously developed for low-intensity tES [23,24,45] - however here we divide scalp into Superficial Scalp (SS) and Deep Scalp (DS) compartments. Skull, meninges, gray matter, and white matter compartments are assigned standard fixed tissue conductivities. Clinical electrode montages are reproduced (e.g. BF) with boundary conditions corresponding to static impedance ($I_n = 1$ mA) and dynamic impedance ($I_n = 900$ mA) testing. (C) For each subject and electrode montage, a volumetric mesh was generated from the segmented data. (D) The model was initialized with a deep scalp conductivity (σ_{DS}) and a maximum superficial scalp conductivity ($\sigma_{\overline{SS}}$). Independently for 1 mA and 900 mA current, an iterative model then computed current flow based on tissue resistivities, updating superficial scalp conductivity ($\sigma_{\overline{SS}}$) in each element based on local electric fields using a transfer function, and then recalculated brain current flow (blue dashed square). The model converges after ~15 k iterations, producing a model prediction of static impedance (for 1 mA) and dynamic impedance (for 900 mA). (E) Model predicted static and dynamic impedance were compared with clinical static and dynamic impedance from the subject. If there was any significant mismatch, the model was reinitialized with updated deep scalp conductivity (σ_{DS}) and a maximum superficial scalp conductivity ($\sigma_{\overline{SS}}$), and the FEM was re-run until convergence (blue dashed square). When model static and dynamic impedance matched clinical data, a patient specific deep scalp conductivity (σ_{DS}) and a maximum superficial scalp conductivity ($\sigma_{\overline{SS}}$) was set.

center of the electrodes ends up approximately 3–5 cm above the canthus of the eye.

2. Right Unilateral (RUL) disk electrode montage: The center of the frontotemporal disk electrode is aligned with the midpoint of an imaginary line between the tragus and lateral canthus of the eye. The bottom of the disk electrode is placed superior to the imaginary line. The superior electrode disk is centered and to the right of the vertex, which is the intersection of imaginary lines from nasion to inion, and the intertragal line.

Stimulation electrodes and gels were modeled in SolidWorks (Dassault Systèmes Corp., Waltham, MA). For the BF montage, we represented ECT adhesive pad electrodes with dimensions of 4.2 × 4.9 cm and thickness of ~1.7 mm, and gel conductivity of 0.018 S/m (based on stand-alone measurements of Thymapad electrodes). For RUL montage we represented circular metal electrodes with a diameter of 5 cm and paste conductivity of 0.018 S/m.

Table 1
Parameters and corresponding values represented in Equation (1).

Parameters	Values
A	$5*10^{-4}$
B	36.15
C	$4.35*10^{-4}$
D	0.015

2.7. Computation and subject specific tissue parameterization

These modeled electrodes and gels were incorporated into the segmentation. Volume meshes were generated from the segmented data and exported to COMSOL Multiphysics 5.5 (COMSOL Inc., MA, USA). The resulting mesh comprised >9,000,000 tetrahedral elements (>15,000,000 degrees of freedom).

The Laplace equation $\nabla.(\sigma\,\nabla\,V) = 0$ (V: scalar electric potential; ∇: gradient vector; σ: conductivity) was solved and the boundary conditions were used such that current in static models (1 mA) and dynamic models (900 mA; unless otherwise stated) is applied to one of the electrode terminals, while the other electrode is grounded. Superficial-scalp conductivity was expressed as a function of electric field (equation (1)). The finite element method (FEM) model was implemented using COMSOL. To converge the solution (Fig. 1 C1), a linear system solver of conjugate gradients was used with a relative tolerance of $1*10^{-3}$ with a nonlinear system solver using the Newton-Raphson method (<500 iterations). This method is applied to millions of degrees of freedom iteratively. Note non-adaptive approaches would require a single Newton-Raphson iteration requiring ~100–500 iteration of the conjugate gradient solver. The total iterations increase to ~2-15 k in the adaptive model involving ~60–100 N-Raphson iterations.

While the computation of electric field, changing scalp conductivity, and then re-computation of electric field is iterative, for

the purpose of our model the result is considered instant (or at least much faster than ECT pulse duration and/or the process by which device measures impedances). Time is not considered. All predictions of impedance and electric field (including in the brain) should be understood as steady state during current application. Effects on the brain are represented directly by electric field, following the quasi-uniform assumption [33,34] without considering non-linear neurophysiological response such as those depending on an electric field threshold [14,35–37] or waveform [38].

For North Shore-Long Island Jewish Health System data including modeled subjects (#21908, #22615, #22035, #21778), static impedances were averaged across the first stimulation of each session, and dynamic impedances were averaged across the sessions where the seizure was generated for every stimulation. An iterative approach (Fig. 1 C2) was used to search for each subject-specific deep-scalp layer conductivity (σ_{DS}) and maximum superficial-layer conductivity ($\sigma_{\overline{SS}}$) such that model static impedance and dynamic impedance matched each subject's clinical values.

2.8. Statistical analysis

Normality test of ECT trial data (static and dynamic impedance) from the New York State Psychiatric Institute, from the North Shore - Long Island Jewish Health System, and from the Medical University of South Carolina was assessed using Lilliefors. Normality of static impedance over instruments, subjects, and time (electrode preparation section) was evaluated with Kolmogorov-Smirnov test. The impedance data that was further transformed in log base 10 (log10) with linear regression indicating the relationships between static impedance and dynamic impedance within and across patients (New York State Psychiatric Institute, North Shore - Long Island Jewish Health System), static impedance and seizure charge threshold, and dynamic impedance and seizure charge threshold (North Shore - Long Island Jewish Health System), the average charge and dynamic impedance (Medical University of South Carolina). Bonferroni post-hoc analysis was performed to correct for multiple comparisons. A Kruskal- Wallis ANOVA determined differences in the static and dynamic impedances, across all subjects and sessions based on differences in pulse width and montage (New York State Psychiatric Institute) and each instrument, subject and time point (electrode preparation section) followed with a post-hoc. Wilcoxon signed rank test was used to compare the dynamic impedances and charge of subjects at 600 and 900 mA (Medical University of South Carolina).

3. Results

3.1. Relation between static impedance and dynamic impedance in single-center ECT trial

While static impedance and dynamic impedance has long been recognized as measures of individual resistance to electroconvulsive therapy (ECT), their etiology, correlation, and consequences – including how they impact on seizure induction – remain a matter of speculation. Practically, an atypically high static impedance may suggest an undesirably high dynamic impedance, and hence the need to correct electrode setup [39](see below). However, such aberrant impedances may be distinct from less extreme and naturally occurring variation in head impedance (e.g. under ideal electrode site preparation). We conducted a retrospective analysis of static impedance and dynamic impedance from 90 patients (with a total of 622 ECT stimulations) from a previously reported clinical trial [16].

ECT data varying montage electrode placement (RUL vs BL) and stimulus waveform (brief pulse vs ultra-brief pulse) were re-analyzed from the New York State Psychiatric Institute trial [16] – importantly for our purposes, other stimulation parameters were reliably controlled and fixed (e.g. device, electrodes, operator experience, preparation technique). Across ECT conditions, dynamic impedance reliably increased with static impedance (Fig. 2) with significant interactions both across subjects within ECT condition and within subject across repeated sessions (not shown). Across stimulation montages and waveforms, there was an evident relationship between static and dynamic impedances (RUL brief: $F(2,19) = 9.99$, $p < 0.05$, $R^2 = 0.345$; BL brief: $F(2,38) = 27.5$, $p < 0.05$, $R^2 = 0.42$; RUL ultra-brief: $F(2,21) = 67.3$, $p < 0.05$, $R^2 = 0.762$; BL ultra-brief: $F(2,22) = 33.6$, $p < 0.05$, $R^2 = 0.604$). All p-values survived the Bonferroni correction. After multiple comparison correction: RUL brief CI: 0.0843–0.8516; BL brief CI:0.3459–0.8281; RUL ultra-brief CI: 0.6569–0.9566; BL ultra-brief CI: 0.4572–0.9192. This analysis shows that when a consistent ECT preparation procedures are followed, a correlation between static impedance and dynamic impedance is evident; this is consistent with some aspect of individual anatomy increasing both static and dynamic impedance.

We further analyzed within-subject variance across ECT sessions in static and dynamic impedance (Fig. 2 error bars). Evaluation of the impact on static impedance and dynamic impedance by subject was modeled using a Kruskal-Wallis (static: $H(87) = 579.47$, $p < 0.001$; dynamic: $H(87) = 472.93$, $p < 0.001$). In a linear regression with subjects as a categorical covariate there was significant within-subject correlation between static and dynamic impedance (significant in 11 of 30 patients with >9 treatment sessions, $p < 0.05$; overall model significant, $p < 0.001$); a post-hoc analysis of covariance was significant ($F(28,352) = 7.07$, $p < 0.001$). Thus, for a given subject, presenting a higher relative static impedance at a given session, a higher relative dynamic impedance is expected. This result can be explained either by differences in tissue (scalp) properties across sessions, or by differences in electrode preparation across sessions (see below). Notwithstanding within subject variance, we confirm difference in both static and dynamic impedances across subjects are reliable across sessions (static impedance [BL brief: $H(23) = 136.58$, $p < 0.001$; BL ultra-brief: $H(39) = 203.57$, $p < 0.001$; RUL brief: $H(21) = 141.49$, $p < 0.001$; RUL ultra-brief: $H(20) = 125.59$, $p < 0.001$], dynamic impedance [BL brief: $H(23) = 91.7$, $p < 0.001$; BL ultra-brief: $H(39) = 165.26$, $p < 0.001$; RUL brief: $H(21) = 141.49$, $p < 0.001$; RUL ultra-brief: $H(20) = 125.59$, $p < 0.001$]). Barring systematic within-subject errors in electrode preparation (e.g., electrodes were always poorly misplaced on given subject), this result combined with analysis of averaged subjects' data (Fig. 2), is consistent with individual differences (anatomy and/or tissue properties) impacting correlation between static and dynamic impedances.

3.2. Impact of electrode preparation technique on static impedance

In a sample of healthy subjects, we measured static impedance across systematically varied adhesive electrode preparation techniques (Fig. 3). Each condition was tested repeatedly across subjects ($n = 3$) and the changes over time were monitored. Static impedance differed among conditions for both instruments (Thymatron: $H(5) = 59.82$, $p < 0.05$; SpECTrum: $H(5) = 63.75$, $p < 0.05$). Post hoc analysis corrected for Bonferroni revealed that static impedance increased in the absence of the adhesive (alcohol skin cleaning only). All electrode preparation conditions using an adhesive solution applied to the electrode surface (Pretac or PVP-K90) resulted in a comparable and minimal static impedance for each given

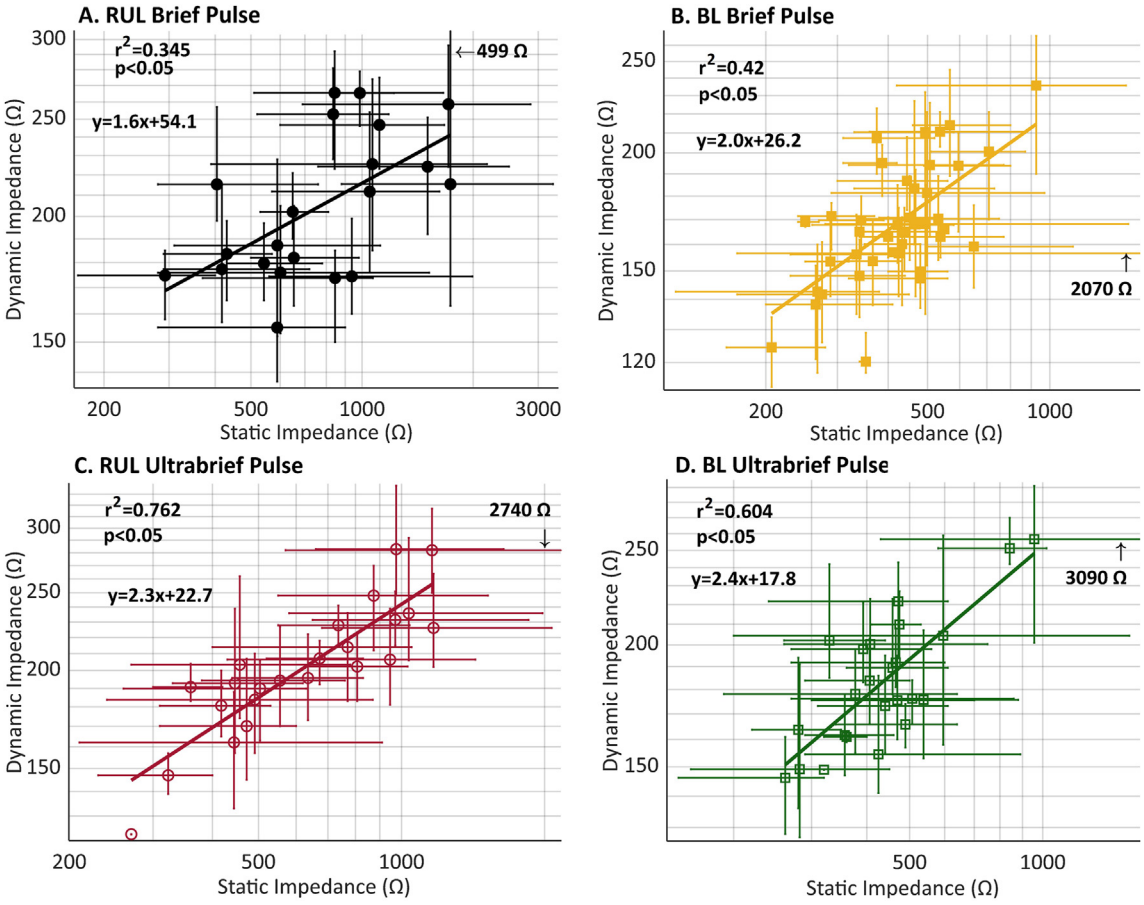

Fig. 2. Retrospective analysis of data from a single center ECT trial comparing RUL and BL electrode placements and brief and ultra-brief pulse stimulation. In a New York State Psychiatric Institute patient sample receiving BF ECT, across (A) RUL Brief Pulse (black), (B) BL Brief Pulse (yellow), (C) RUL Ultrabrief Pulse (red), and BL Ultrabrief pulse (green) there was a significant correlation between patient static impedance and dynamic impedance. The average impedance across sessions is represented for each subject as well as the full range of variance (error bars).

subject. Reduction in electrode contact area by 50 % increased static impedance a factor of ~1.5–2.7 (Fig. 3).

Static impedance measures by the SpECTrum were greater than Thymatron at each time point (time = 0: H (1) = 13.0124, $p < 0.001$; mean difference, 12.67 +- 6.88, $p < 0.001$; time = stable: H (1) = 17.7067, $p < 0.001$; mean difference, 14.78 +- 6.88, $p < 0.001$) reflecting how each device uniquely probes and calculates static impedance. Static impedance measures decreased significantly over time for all subjects, conditions, and instruments (H (1) = 5.38, $p < 0.05$). Additionally, difference was observed across all subject pairings for each device, besides the pairing of Subject 1 and Subject 3 on the SpECTrum (Thymatron: s1, s2: H (1) = 61.0792, $p < 0.001$; s1, s3: H (1) = 30.3514, $p < 0.001$; s2, s3: H (1) = 17.4964, $p < 0.001$; SpECTrum: s1, s2: H (1) = 31.6038, $p < 0.001$; s1, s3: H (1) = 3.4103, $p = 0.065$; s2, s3: H (1) = 21.728, $p < 0.001$), consistent with subject anatomy/tissue properties impacting static impedance.

Even under our tightly controlled experimental conditions and with optimal preparation (use of adhesive), moderate variability was observed between repetition trials. Under realistic clinical conditions, variability both in the quantity (area coverage) and quality (e.g. extent of adhesion) of electrodes could produce substantial impedance variance. Nevertheless, this supports our modeling analysis where difference between individuals is not dominated by idiosyncrasy in the quality of electrode-skin contact (i.e. as models assume complete electrode-skin contact) but rather reflects subject's head properties.

3.3. Development of individualized adaptive tissue models of ECT

Previously MRI-derived head models to predict subject-specific brain current flow were developed [24,40] and validated [41,42] for low-intensity tES, such as tDCS, and then subsequently applied to ECT [14,43]. These models assumed non-adaptive tissue resistivity. Here we developed a novel ECT modeling pipeline (Fig. 1) with adaptive tissue conductivity, such that local scalp conductivity changes with electric field strength (Fig. 4). The analysis was conducted on data from four ECT patients from the North Shore-Long Island Jewish Health System. Each patient's anatomical MRI was segmented and an iterative search process identified the maximum superficial scalp conductivity ($\sigma_{\overline{SS}}$) and the deep scalp conductivity (σ_{DS}) that produced a prediction of static and dynamic impedance values corresponding to the patient's clinical data. The resulting subject specific parameters were: Subject 21908, $\sigma_{\overline{SS}} = 0.16$ S/m at $E_{\overline{SS}} \geq 403$ V/m, $\sigma_{DS} = 0.002$ S/m; Subject 22615, $\sigma_{\overline{SS}} = 0.5$ S/m at $E_{\overline{SS}} \geq 1185$ V/m, $\sigma_{DS} = 4.5*10^{-4}$ S/m; Subject 22035, $\sigma_{\overline{SS}} = 0.3$ S/m at $E_{\overline{SS}} \geq 725$ V/m, $\sigma_{DS} = 0.008$ S/m; Subject 21778, $\sigma_{\overline{SS}} = 0.4$ S/m at $E_{\overline{SS}} \geq 955$ V/m, $\sigma_{DS} = 0.0012$ S/m.

Stimulation with 1 mA (Fig. 4, static model) produced peak scalp electric fields under and around electrode edges (>80 V/m) with moderate increases in conductivity (~0.03 S/m) around the electrode perimeters. Stimulation with 900 mA (Fig. 4, dynamic model) produced high electric fields across the scalp forehead with peaks

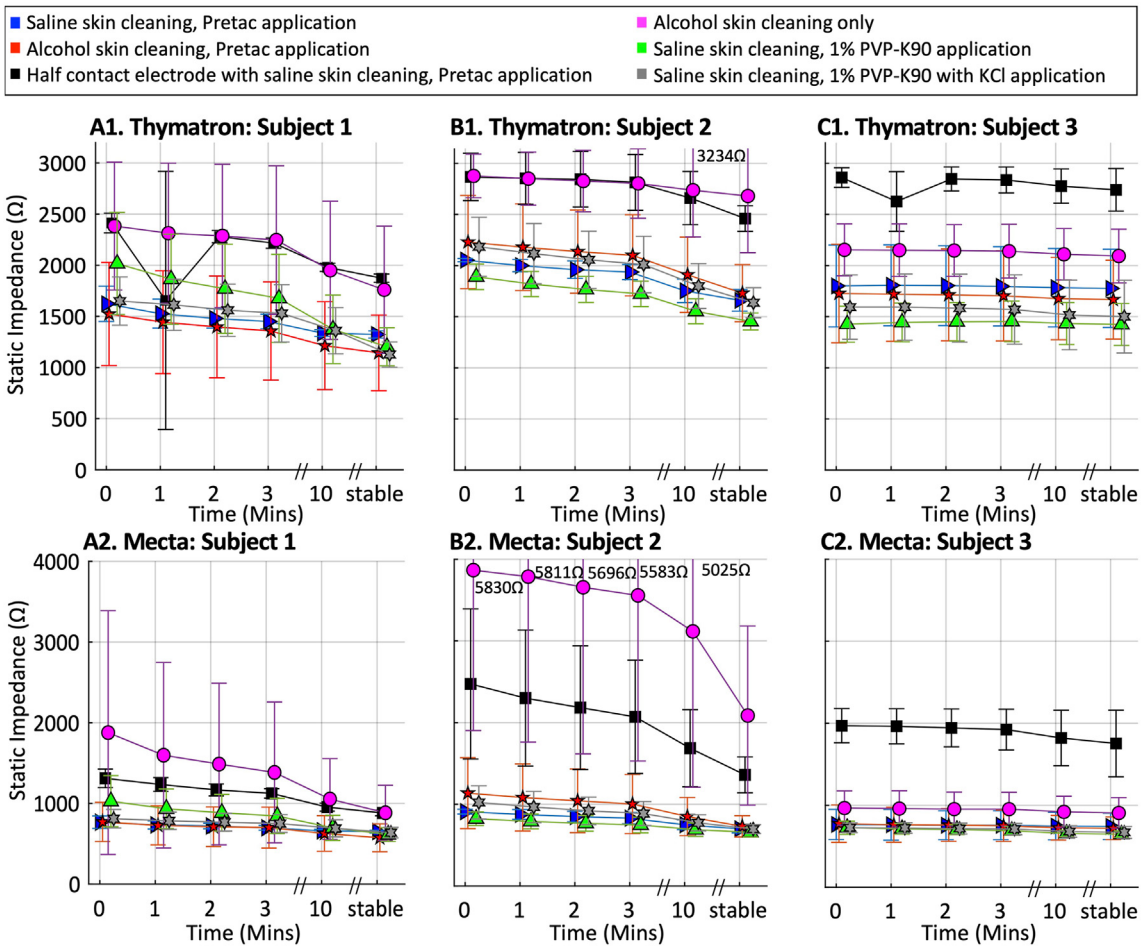

Fig. 3. Static impedance over time under six electrode preparations. Repeatedly across three subjects (mean ± S.D.) and both the Thymatron (A1, B1, C1) and SpECTrum (A2, B2, C2) devices, static impedance was measured under varied electrode preparation techniques. Prior to electrode placement the skin was gently cleaned with either isotonic saline or alcohol (99 %) and allowed to dry. Thymapads electrodes were lightly coated with Pretac, polyvinylpyrrolidone (PVP) with or without KCl, or not at all, before being placed on the skin. Static impedance was measured immediately after electrode application (t = 0) and at every minute until a stabilized.

around electrodes (>4500 V/m), and an associated increase in scalp conductivity (0.15–0.5 S/m). The resulting brain current flow during ECT also predicted peak electric fields >490 V/m.

3.4. Adaptive scalp response and the relation between static and dynamic impedance

The role of head anatomy in ECT outcomes remains unclear, and is complex to understand experimentally when gross anatomy, tissue properties, and neurophysiology all vary across individuals. The role of gross anatomy can be considered using computational models by 1) fixing head anatomy and manipulating tissue (scalp) properties; or 2) artificially changing (e.g. dilating) a single anatomical layer (scalp). These approaches are used first to explain the relation between dynamic and static impedance, and then how they impact delivery of current to the brain.

For each head we fitted deep-layer scalp conductivity (σ_{DS}) and maximum superficial-layer scalp conductivity ($\sigma_{\overline{SS}}$). Subsequently, it is possible to examine the role of scalp properties by simulating the "swapping" of the scalp properties across different heads (Fig. 5). Starting from a base set of four head anatomies (Subject 22615, square; Subject 21778, diamond; Subject 22035, circle; Subject 21908, x with corresponding σ_{DS} and $\sigma_{\overline{SS}}$ for each subject), we then swapped (mixed) scalp properties across heads (colors), resulting in 60 synthesized heads (plus the 4 originals). Under an assumption that a theoretical subjects head anatomy, deep-layer scalp conductivity (σ_{DS}) and maximum superficial-layer scalp conductivity ($\sigma_{\overline{SS}}$) can vary independently, each synthesized head represented a novel hypothetical subject. This approach allows systematic comparison of the relative impact of anatomy and scalp properties to ECT outcomes as predicted by the synthetic models.

The relationship between static impedance and dynamic impedance is evident though imperfect (Clinical BF: $F(2,15) = 5.84$, $p < 0.05$, $R^2 = 0.28$) in the North Shore-Long Island Jewish Health System clinical BF ECT series (Fig. 5 A). The predicted relationship between static impedance and dynamic impedance across all the synthetic heads was complex (Fig. 5 B) though interactions are evident when considering individual head anatomy (Fig. 5 B1, B2, B3, B4) or a given $\sigma_{\overline{SS}}$ (Fig. 5 C1, C2, C3, C4).

Thus, simulations with swapped-scalps predict that variation in scalp properties are relatively more important than gross anatomy in determining static impedance and dynamic impedance. Specifically, extreme variations in static impedance and dynamic impedance are governed by $\sigma_{\overline{SS}}$ and σ_{DS} respectively. Therefore, because $\sigma_{\overline{SS}}$ and σ_{DS} vary independently a dispersion of static and dynamic conductivities is produced. A weak interaction persists because σ_{DS} has (in addition to a strong effect on static impedance) a weak effect on dynamic impedance (Fig. 5 B1, B2, B3, B4 lines

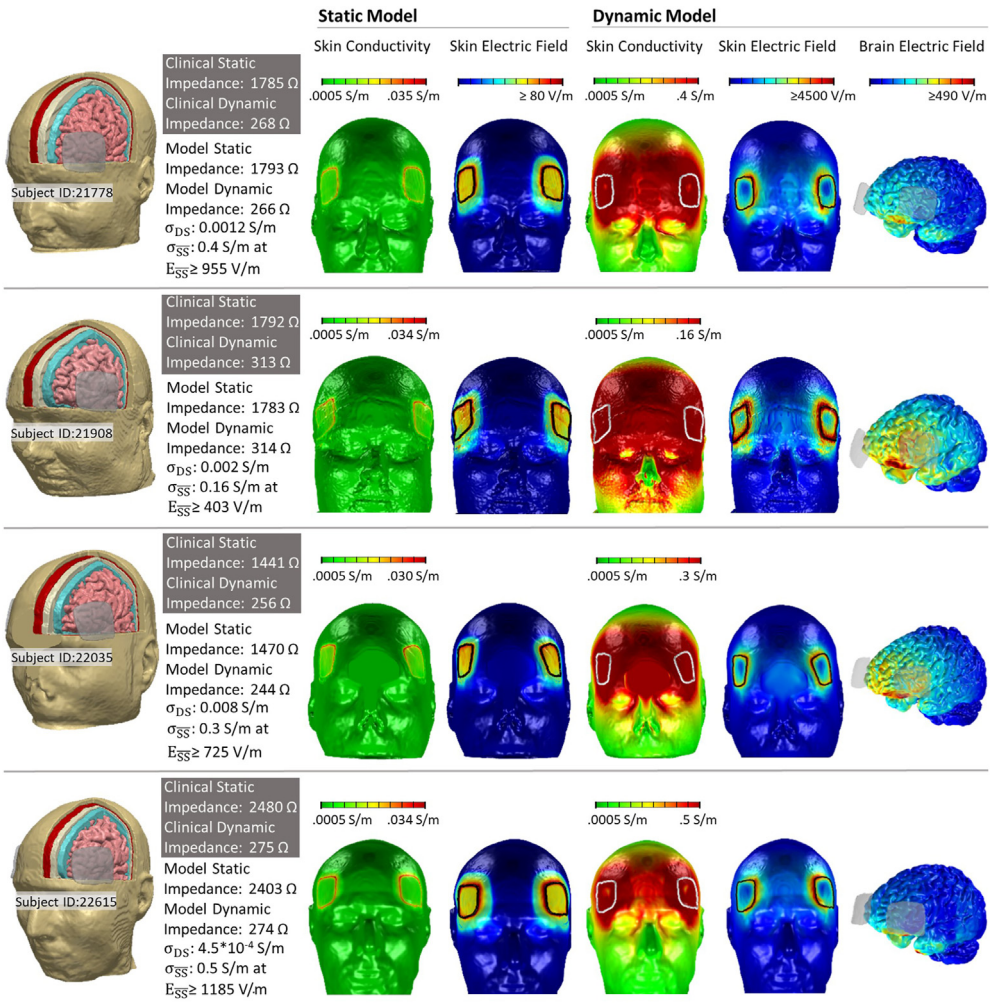

Fig. 4. Dynamic ECT models for four ECT subjects. Dynamic FEM models simulated current flow across four subjects who have received ECT (Subject IDs: 21778, 21908, 22035, 22615). (First Column) Models anatomy was based in subject anatomical MRI. Static impedance and dynamic impedance values were recorded for each subject (gray box). Each subject model was assigned a specific deep scalp conductivity (σ_{DS}) and a maximum superficial scalp conductivity ($\sigma_{\overline{SS}}$) as indicated, such that adaptive FEM simulation predicted corresponding static impedance (based on 1 mA applied current) and dynamic impedance (based on 900 mA applied current) as indicated. (Second and Third Column) Results from the static impedance (1 mA current) simulation showing resulting superficial scalp conductivity and scalp electric field. (Third, Fourth, Fifth Column) Results from the dynamic impedance (900 mA current) simulation showing resulting superficial scalp conductivity, scalp electric field, and brain electric field. We emphasize in these novel adaptive simulations that brain current flow was determined by tissue conductivity, superficial scalp conductivity was simultaneously determined by local electric field. Even for the 1 mA (static) model local changes in scalp conductivity are predicted. For the 900 mA (dynamic) model, the saturation of the transfer function between superficial scalp electric field and conductivity results in a more diffuse saturation of scalp conductivity (front of head) compared to scalp electric field (around electrodes).

represent fixed head and $\sigma_{\overline{SS}}$, so only σ_{DS} varying). Head anatomy moderate both static and dynamic impedance (see also below). The importance of deep-layer scalp (σ_{DS}) conductance, with head anatomy as a moderator, on static impedance is evident when noting that for a given head and σ_{DS}, static impedance is nearly fixed, despite variation in dynamic impedance. This vertical dispersion is also why a relationship between static and dynamic impedance is not evident across swapped-scalp models (e.g. for static impedance >2600 ohm a wide range of dynamic impedance is possible). For a given superficial-layer scalp conductivity ($\sigma_{\overline{SS}}$), as anatomy and deep-layer scalp conductivity (σ_{DS}) varied, correlation between static impedance and dynamic impedance increased with decreasing $\sigma_{\overline{SS}}$ (Fig. 5 C1, C2, C3, C4).

Thus, we predict the degree of correlation between static impedance and dynamic impedance expected in any data set would be limited by conditions (montage, waveform) or individuals which increase the contribution to dynamic impedance of high superficial-layer scalp conductivity ($\sigma_{\overline{SS}}$) compared to deep-layer scalp conductivity (σ_{DS}). Meaning, it is the same adaptive dynamic scalp conductivity properties that result in reduced dynamic impedance compared to static impedance, that introduce variability in the scale of reduction and so therefore, correlation between static and dynamic impedance.

Across (almost all) variations in tissue properties, the relative (rank) order of dynamic impedance was fixed (from higher to lowest: Subject 22615, square; Subject 21778, diamond; Subject 22035, circle; Subject 21908, cross). Across variation in adaptive-tissue properties, the rank order of static impedance was not consistent across heads, though some trends were evident. Subject 22035 presented the lowest relative static impedance. Subject 22615 presented the highest relative static impedance. In any case, neither rank order for static impedance or dynamic impedance corresponded to the rank order of any global anatomical feature

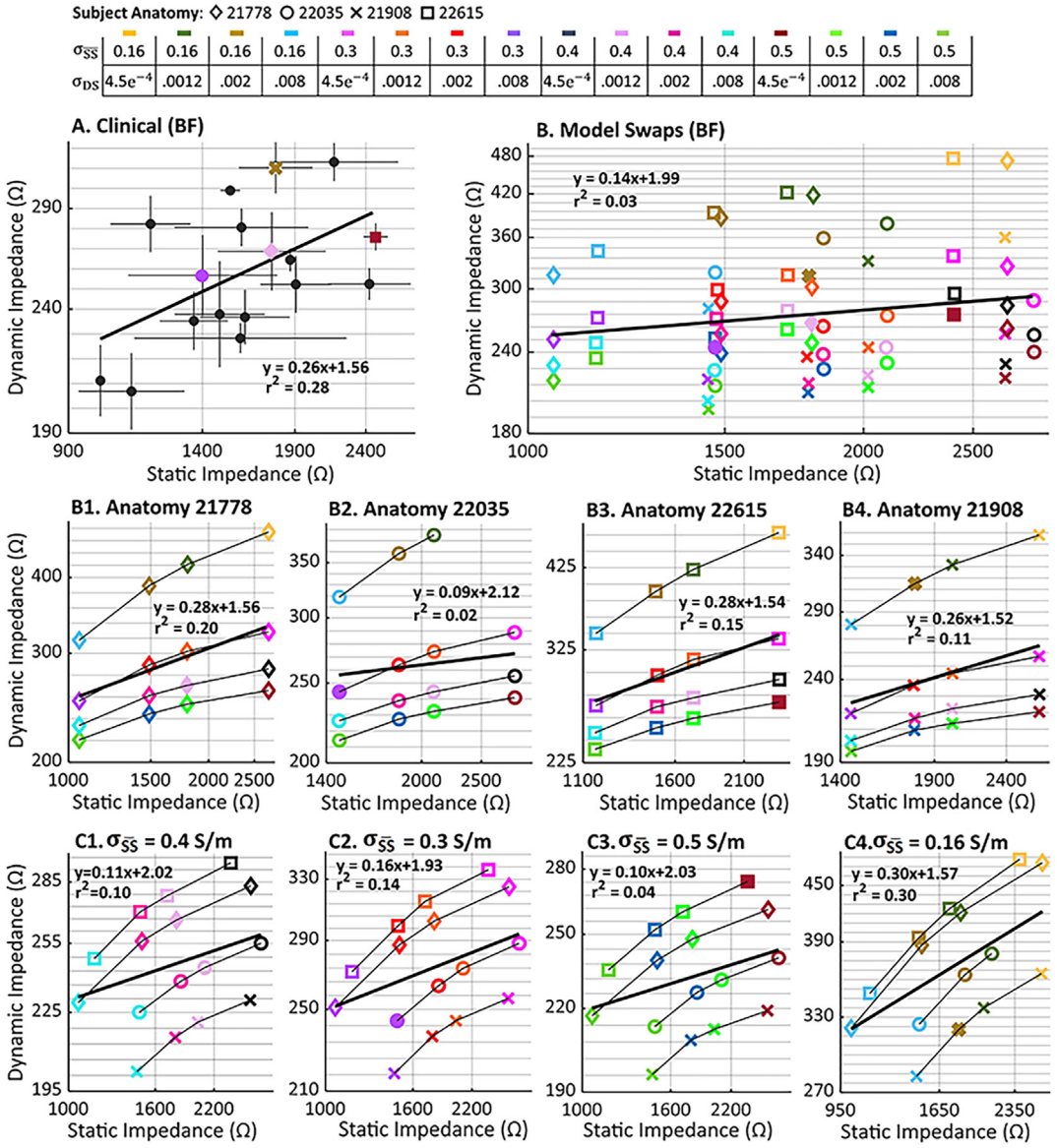

Fig. 5. Relation between Dynamic Impedance and Static Impedance in clinical data and adaptive models including scalp swaps. (A) Dynamic impedance and static impedance were modestly correlated in North Shore-Long Island Jewish Health System patient sample receiving BF ECT (mean ± S.D.). Four subjects (colored symbols) were selected for adaptive FEM simulation. (B) In these four subjects, static and dynamic impedance values were simulated by assigning subject specific deep scalp conductivity (σ_{DS}) and a maximum superficial scalp conductivity ($\sigma_{\overline{SS}}$). The conductivities (in S/m) are called "endogenous" for our purposes here (Subject 22035 $\sigma_{DS} = 0.008$, $\sigma_{\overline{SS}} = 0.3$; Subject 21778 $\sigma_{DS} = 0.0012$, $\sigma_{\overline{SS}} = 0.4$; Subject 21908 $\sigma_{DS} = 0.002$, $\sigma_{\overline{SS}} = 0.16$; Subject 22615 $\sigma_{DS} = 4.5{*}10^{-4}$, $\sigma_{\overline{SS}} = 0.5$). In scalp swaps, all deep scalp conductivity (σ_{DS}) and a maximum superficial scalp conductivity ($\sigma_{\overline{SS}}$) were varied across all subject anatomies, resulting in 64 simulates swapped-conductivity heads (including the endogenous 4 heads). For each head, static impedance and dynamic impedance was predicted using our adaptive pipeline. There was only a weak correlation between simulated static and dynamic impedances. (B1, B2, B3, B4) Replotting the same model swap results but categorized by subject anatomy. Note, for a given head anatomy and a given deep scalp conductivity (σ_{DS}), varying superficial scalp conductivity ($\sigma_{\overline{SS}}$) changes dynamic impedance but not static impedance. This vertical distribution of dynamic impedances for a given static impedance reduces overall correlation, even within a single anatomy. For a given head anatomy and superficial scalp conductivity ($\sigma_{\overline{SS}}$), decreasing superficial scalp conductivity ($\sigma_{\overline{SS}}$) monotonically increases both static impedance and dynamic impedances, explaining the source of overall correlation. (C1, C2, C3, C4) Replotting the same model swap result but categorized by a given $\sigma_{\overline{SS}}$ for all subjects. Note, correlation between static and dynamic impedances increases with the decrease in superficial scalp conductivity ($\sigma_{\overline{SS}}$), consistent with changes in superficial scalp conductivity reducing overall correlation.

(head circumference, skull thickness, inter-electrode distance). This suggested that it is not possible to predict (relative) static or dynamic impedance based on any simple anatomical measure (consistent with clinical observations [5]).

The salient result here is not that our adaptive modeling approach can match the clinical impedance data, since adjusting subject $\sigma_{\overline{SS}}$ and σ_{DS} (Fig. 5) could ensure model approximation of subject-specific clinical data. Rather, these models provide a framework to explain clinical observations and reconcile incongruent findings (see Discussion).

3.5. Adaptive scalp response and the relation between brain current intensity and static or dynamic impedance

In the North Shore- Long Island Jewish Health System BF ECT clinical series, there was no evident relation between static

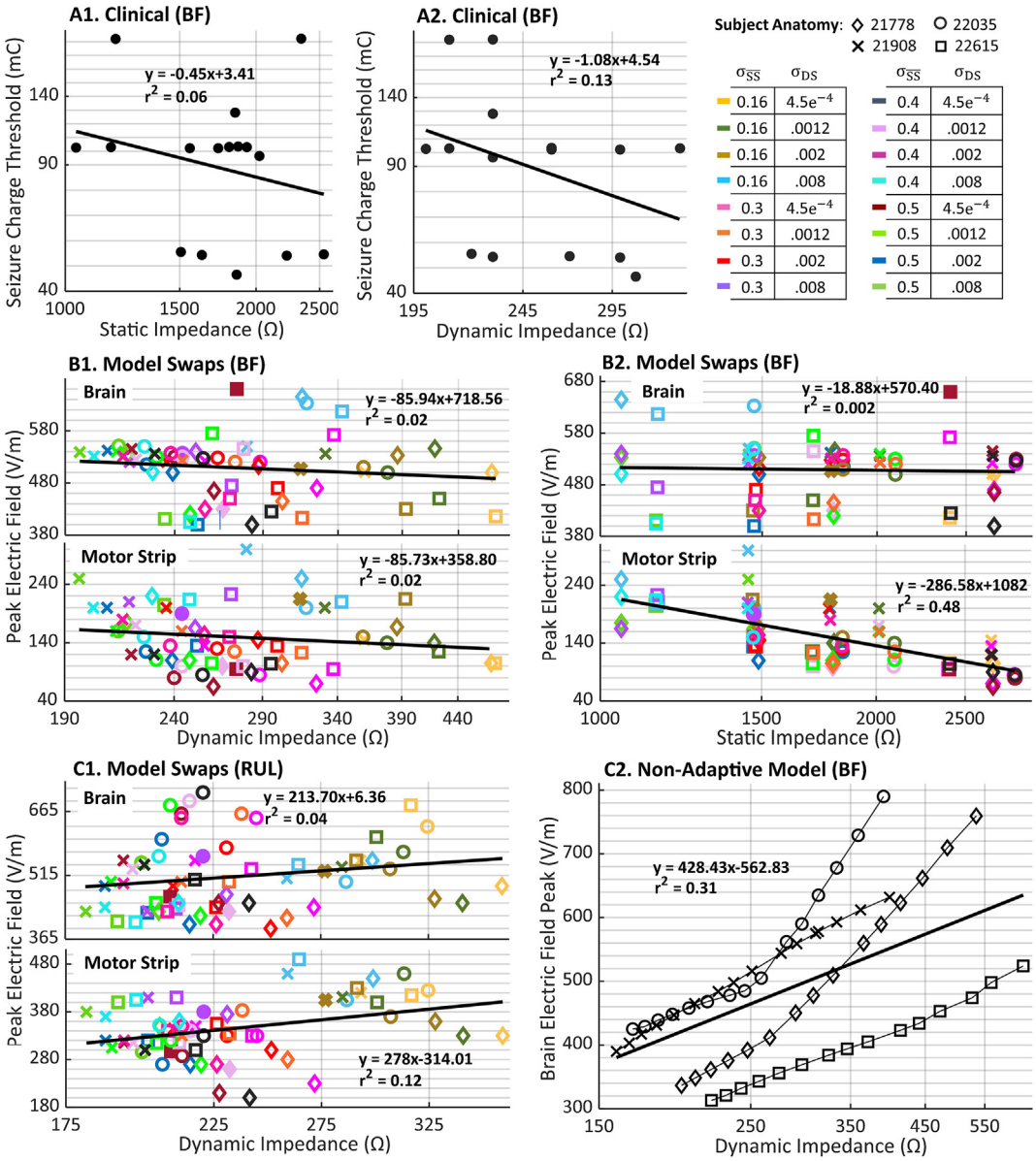

Fig. 6. Relation between brain electric field (or seizure threshold) in clinical data and adaptive scalp models including scalp swaps. In theory, conditions that result is higher electric fields (at the region of seizure initiation) will be associated with reduced charge required to trigger a seizure, i.e. lower seizure threshold. (A) In a North Shore-Long Island Jewish Health System patient sample receiving BF ECT, the relation between increasing static impedance (A1) or increasing dynamic impedance (A2) and decreasing charge threshold for seizure initiation. (B) The predicted relation between brain electric field and dynamic impedance (B1) or static impedance (B2) can be simulated for the BF electrode montage using adaptive FEM models of the 64 swapped-conductivity heads (including the endogenous 4 heads). Brain wide peak electric field is considered (higher panel) as well as motor strip peak electric field (lower panel). Note: In both cases (B1, B2), the electric field represented is for the applied 900 mA case. Only weak correlations are predicted, with the strongest correlation (negative direction) for the case of static impedance and motor strip peak electric fields. (C1) Using adaptive FEM modeling, the relation between dynamic impedance and static impedance was further predicted in same heads for the RUL electrode montage. Weak correlation was predicted, with the strongest relationship (positive direction) for dynamic impedance and motor strip peak electric field. (C2) Conventional (non-adaptive tissue) FEM of the four anatomical head, where for each uniform scalp conductivity was varied to adjust dynamic impedance, predicted quasi-linear relationship for each head between dynamic impedance and brain electric field. Variability between heads resulted in a weaker group correlation between dynamic impedance and brain electric field. We note the prediction in non-adaptive conventional stimulation of increasing electric field with increased dynamic impedance is expected. While the predictions from adaptive FEM suggest a more complex and nuanced relationship between dynamic impedance and electric field (and so charge needed to produce seizures).

impedance and seizure charge threshold (Fig. 6 A1) or dynamic impedance and seizure charge threshold (Fig. 6 A2). Both comparisons were not statistically significant at $p < 0.05$ (A1. Clinical BF: F (2,14) = 0.84, p = 0.375, R^2 = 0.0566; A2. Clinical BF: F (2,14) = 2.07, p = 0.172, R^2 = 0.129). Across the swapped BF head model stimulations (4 originals plus 60 synthesized scalp heads), we predicted peak electric fields, both brain-wide and specifically in the motor strip. There was no evident correlation between static (Fig. 6 B1) or dynamic (Fig. 6 B2) impedance, and brain-wide peak electric field or motor strip electric field. The exception between a negative relation between static impedance and motor strip peak electric field.

While these adaptive models were parametrized based on BF ECT data, we used the same swapped heads to predict the relation

between static impedance or dynamic impedance and brain current delivery for RUL ECT (Fig. 6 C1). Relationships were weak, and trended positive. We further considered non-adaptive models in order to highlight the unique behavior of adaptive models (Fig. 6 C2). In non-adaptive models, for each subject head, the (uniform) scalp conductivity was incrementally decreased, producing a range of impedance (note, in these non-adaptive models we distinguish static impedance or dynamic impedance). As expected, in non-adaptive models, brain electric field increased monotonically for each subject with increased impedance. This slope varies across heads but remains significant across the group.

MRI-derived head models can be artificially altered [44] including dilation of specific tissue layers [25,45]. Keeping tissue conductivity properties fixed (as optimized for each subject), we first dilated only superficial scalp layer by ~6x (Fig. 7, middle row). Superficial-scalp dilation increased static impedance, decreased dynamic impedance, and decreased brain current delivery in all four heads. Further dilation of deep scalp layer by ~2x (Fig. 7, bottom row) increased static impedance in three of the four heads, increased dynamic impedance in all four heads, and decreased current delivery in three of the four heads in comparison with the results from superficial-scalp dilation. Notably, these simulations show a dissociation among static impedance, dynamic impedance, and electric field in the sense that specific changes can affect them relatively differently (Table 2). This also reinforces the unique outcomes, and so value, of adaptive-resistivity models.

3.6. Response to moderated ECT voltage and current: Model validation against classical clinical data

While modern ECT uses currents of 800–900 mA, in two earlier trials the current and/or voltage of ECT was systematically varied within subjects, which can also be modeled with adaptive-conductivity simulations (Fig. 8 A and Fig. 8 B). Dynamic impedance as a function of voltage from Umlauf et al., 1951 and Maxwell et al., 1968, and dynamic impedance as a function of current for Umlauf et al., 1951 were replotted for each individual subject (gray lines) and group average (yellow Maxwell et al., 1968; black Umlauf et al., 1951). Group data are fit by a power law:

$$R = a\left(V^b\right) \tag{2}$$

$$R = a\left(I^b\right) \tag{3}$$

where R is Dynamic Impedance (in Ohms), V is voltage applied (in Volts), I is current applied (in mA) and a and b are constants.

Alongside these clinical data, results from reducing the applied voltage and current in our adaptive-conductivity models heads is shown and fit to power law. The models broadly reproduce the power law relationship for decreased ECT intensities (100–900 mA). Noting these models were parameterized based only on static (1 mA) and dynamic (900 mA) clinical data. Absolute matching of parameters (a, b) is not expected given the difference

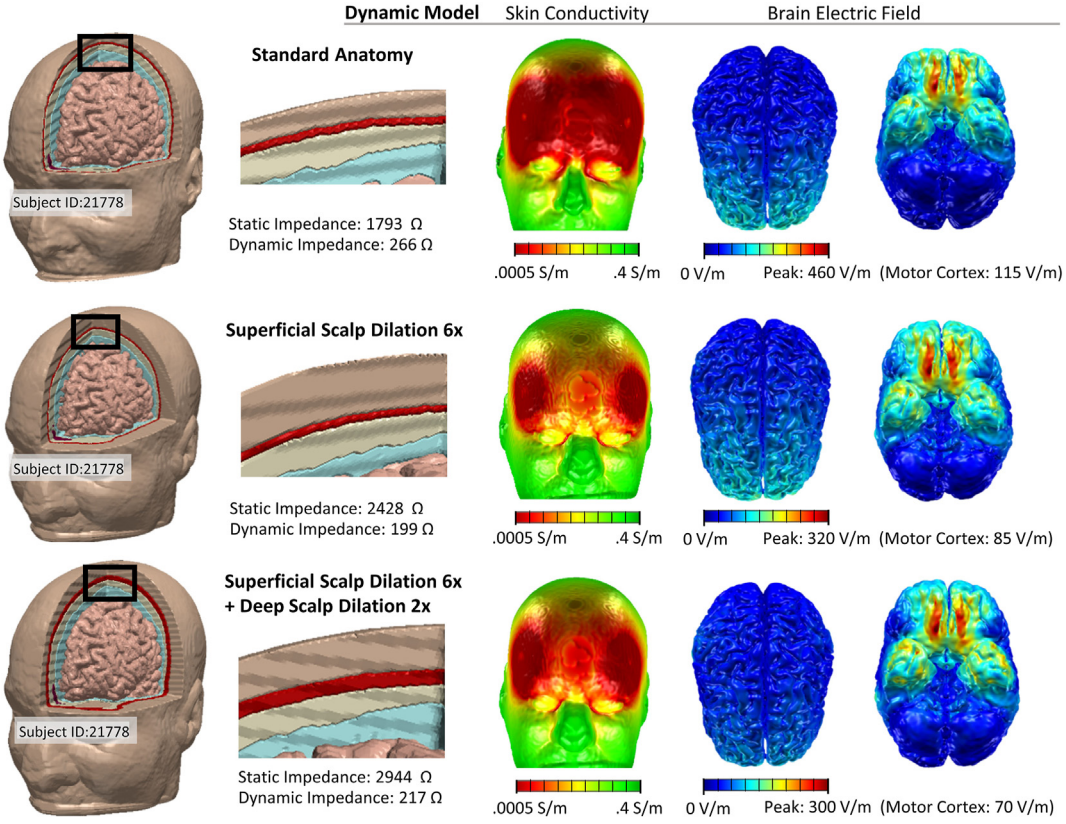

Fig. 7. Tissue Dilation in Adaptive FEM model of ECT, and relationship between static impedance, dynamic impedance, and brain electric field. Our adaptive FEM models suggest a complex relationship among head anatomy, tissue properties, and resulting current flow and resistance. In addition to allowing variance of just select tissue conductivity, computational models can access the role of isolated anatomy, including through superficial tissue dilation [25]. We considered standard (original) anatomy (top row), dilating superficial scalp 6-fold (middle row), and further dilating deep scalp 2-fold (bottom row). In the last case, dilated deep scalp replaces overlying superficial scalp. Compared to the standard anatomy, dilating superficial scalp 6-fold increased static impedance, decreased dynamic impedance, and decreased brain electric field. Further dilating deep scalp 2-fold, increase static impedance, increase dynamic impedance, and decreased further brain electric field. These adaptive FEM simulations show a subtle non-monotonic relationship between static impedance, dynamic impedance, and brain electric fields.

Table 2
Tissue dilation in adaptive FEM stimulation of four ECT subjects. Static/dynamic impedance along with brain/motor electric field from adaptive computational simulations for each endogenous head before and after tissue dilations. These values are indicated for each head's standard (original) anatomy (third column), dilation of superficial scalp 6-fold (fourth column), and further dilation deep scalp 2-fold (last column). Electric field values are for 900 mA and reported as overall peaks in the brain as well as the motor cortex as a region of interest.

	Subject ID	Standard Anatomy	Superficial Scalp Dilation 6x	Superficial Scalp Dilation 6x + Deep Scalp 2x
Static/Dynamic Impedance	#22615	2403/274 (Ω)	2931/206 (Ω)	3820/219 (Ω)
	#21778	1793/266 (Ω)	2428/199 (Ω)	2944/217 (Ω)
	#21908	1783/314 (Ω)	2453/262 (Ω)	2742/295 (Ω)
	#22035	1440/244 (Ω)	2151/199 (Ω)	2083/216 (Ω)
Brain/Motor Electric Field for Dynamic Models	#22615	660/95 (V/m)	411/68 (V/m)	463/64 (V/m)
	#21778	460/115 (V/m)	320/85 (V/m)	300/70 (V/m)
	#21908	507/215 (V/m)	438/150 (V/m)	413/120 (V/m)
	#22035	470/160 (V/m)	400/140 (V/m)	380/115 (V/m)

in protocols. Umlauf et al., 1951 and Maxwell et al., 1968 used sinusoidal stimulation while our models were parameterized based on rectangular pulse trains; It is known that impedance will vary with pulse/sinusoidal waveforms [46].

For non-adaptive models with fixed scalp conductivity, there is a (trivial) linear relationship between applied current and brain electric field [47]. Because scalp impedance may impact delivery of electric field to the brain, we speculated adaptive-models changing impedance with current intensity would result in a non-linear relation between ECT pulse intensity and brain electric field. However, we did not observe a significant deviation from basic linearity (Fig. 8 C and 8 D).

Contemporary data from the Medical University of South Carolina BF/RUL clinical ECT series were analyzed (Fig. 8 E). Subjects received either BF or RUL ECT with circular disk electrodes on MECTA device using 600 mA and 900 mA. For 900 mA ECT, but not 600 mA ECT, subject treatment charge was significantly correlated with dynamic impedance: $F(2,6) = 10.1$, $p < 0.05$, $R^2 = 0.628$. There was no significant difference in charge between 600 mA and 900 mA ECT (Wilcoxon signed rank test, $Z = -0.70$, $p = 0.54$). There was a significant decrease in dynamic impedance from 600 mA to 900 mA ECT (Wilcoxon signed rank test, $Z = -1.96$, $p = 0.02$), which was reproduced in the adaptive models (Fig. 8 E).

4. Discussion

Current passage through the scalp (skin) depends on numerous layers and ultra-structures, each with a complex (non-linear, time-dependent) impedance to current flow [18,48–52] – which is computationally intractable for tES head models [23]. The pipeline developed here to simulate adaptive-scalp conductivity during tES represent two scalp layers, with just two respective associated subject-specific parameters: a deep-scalp layer with fixed conductivity (σ_{DS}) and a superficial-scalp layer where electric fields increase conductivity up to a maximum ($\sigma_{\overline{SS}}$). Ongoing modifications and refinements of our pipeline are welcome (see below) but we suggest the relevance of adaptive-scalp conductivity should be considered in efforts to inform tES/ECT with computational models.

The physical properties of the ECT stimulus markedly effect both efficacy and cognitive side effects. It is the combination of ECT dose (electrode montage, waveform, and stimulus intensity) and head resistive features, that determine how much and where current is delivered to the brain. That head resistivity varies across subjects has been known for decades based on clinical measurement of static impedance and dynamic impedance. But it has been hard to explain if and how these head resistances impact on stimulation during ECT (brain current delivery) because their etiology is unclear. The ongoing universal reliance on static impedance and dynamic impedance in ECT stems largely from limitations built into ECT devices (e.g. voltage compliance) and clinical standards (e.g. preparation quality control) [10] and thus consider only impedance extremes. Nonetheless, there has been discussion spanning decades on whether less extreme variation in impedance parameters (deriving from endogenous difference in anatomy) can be better leveraged to understand and optimize ECT dosing and behavioral outcomes. Our adaptive-conductivity ECT models make a range of predictions on these matters.

Supporting our analysis, we consider data from ECT treatments using a range of devices, electrode placement, and waveforms/pulse widths (Fig. 2, Fig. 5, Fig. 6, Fig. 8) showing a definitive but imperfect relationship between static and dynamic impedance - consistent with endogenous differences between subjects increase static and dynamic impedance together. We also show static impedance is impacted by electrode preparation technique (including both electrode-skin contact area and adhesion quality), but endogenous individual difference remains (Fig. 3).

Adaptive ECT models predict that individual difference in static and dynamic impedance largely reflect difference in individual scalp properties, with head anatomy playing a moderating role. A component of individual scalp conductivity that is insensitive to current passage (σ_{DS}) governs static impedance (to low currents). Though limited scalp conductivity changes are predicted even at low current (Fig. 4), they do not meaningfully impact static impedance (Fig. 5). Dynamic impedance (to high current) is largely governed by the individual's maximum adaptive scalp conductivity ($\sigma_{\overline{SS}}$) in response to current passage, with a smaller influence of the current-insensitive scalp impedance (σ_{DS}). The dual impact of individual σ_{DS} may explain an intrinsic but imperfect relationship between static impedance and dynamic impedance. Contrariwise, the insensitivity of static impedance to the scalp adaption to current flow ($\sigma_{\overline{SS}}$) explains the weakness of any relationship between static and dynamic impedance. Namely, variations in just $\sigma_{\overline{SS}}$ result in the same static impedance being associated with a wide range of possible dynamic impedance. If a given clinical trial reports a correlation between static and dynamic impedance (Fig. 1) or not [5] can reflect difference in electrode/skin preparation or stimulation current. Protocol (e.g. montage, waveform) and subject (e.g. age, sex) differences in impedance would also depend on these scalp properties [9,53].

While static and dynamic impedance are ubiquitously available ECT measures supporting model validation (Fig. 8), tES current flow models have *translational* value only in informing treatment protocols [1,32,35,43,54,55]. These efforts consider the electric fields generated across the brain relevant for both seizure threshold and side-effects. While non-adaptive models predict a direct relation between impedance and brain electric field intensity (Fig. 6 C2),

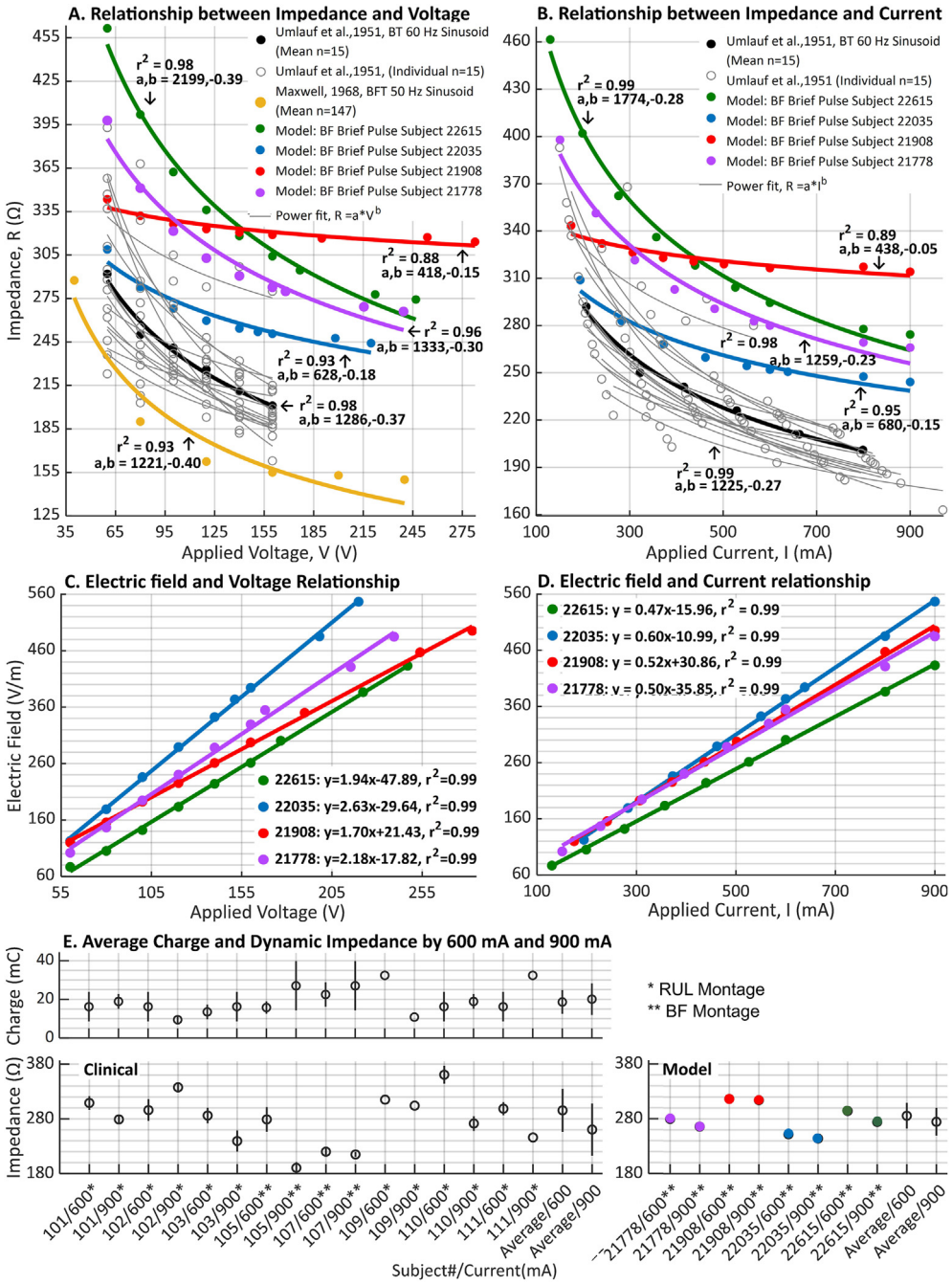

Fig. 8. Relationships between varied applied voltage or current in ECT and measured dynamic Impedance: clinical and modeling results. While in conventional ECT the current level if fixed, in historical experiments the current and/or the voltage was reduced while monitoring dynamic impedance. In Umlauf et al. (1951), ECT dosage (using 60 Hz sinusoidal waveforms, BT electrode montage) was varied, with resulting impedance reported as a function of both applied voltage (A) and applied current (B) [5]. Individual subject data (gray) is reported, alongside group average (black). In Maxwell et al. (1968), the voltage of ECT (using 50 Hz sinusoidal waveform, BFT electrode montage) was reported against dynamic impedance (group average only, yellow) [11]. Using adaptive FEM, for each head (Subject IDs: 21778, 21908, 22035, 22615), we systematically varied the current intensity applied in the model and simulated the resulting dynamic impedance (B) while also reporting the associated voltage (A). Average clinical data and individual model data were fit by a power law. While absolute difference between clinical cases and models are expected (e.g. given variation in protocol and the dependence of conductivity on waveform), the power law fits well the clinical and modeling data. Noting the significant decrease in change in impedance (reflecting decrease scalp resistivity) with increasing voltage/current, we predicted the associated peak brain electrical fields. Increasing voltage (C) or current (D) increased brain electric field in linear manner. Our adaptive-conductivity models show linear relation between electric field and applied voltage and applied current. (E) In a Medical University of South Carolina ECT patient series, stimulation intensity was varied between 600 and 900 mA, with associated seizure thresholds and dynamic impedances reported. Predictions of dynamic impedance from the endogenous adaptive models at 600 and 900 mA are also shown.

adaptive models suggest a complex relationship (Fig. 6 B). Indeed, adaptive ECT models predict a non-monotonic relationship between static impedance, dynamic impedance, and brain currents (Fig. 7). Nevertheless, understanding how adapting scalp properties impact (unmeasurable) brain current flow and how they are reflected in (measurable) impedance parameters, may support efforts to optimize ECT therapy.

There are several challenges and limitations in informing ECT with computational models. Static impedance is device specific (Fig. 3) and there may be differences in ECT dosing, so precise models could be instrument specific. ECT is conventionally titrated through number of pulses/frequency rather than intensity, so computational models may explicitly model seizure-genesis by considering stimulation waveform [36,38,56]. The value of additional modeling details including supplementary tissues [57], electrode and skin interface properties [58,59], scalp ultrastructures [21,48] or conductivity anisotropy [13], should be balanced against the cost of complexity [60] when developing *translational* approaches. Time may also be explicitly considered [18], for example changes in dynamic impedance during a pulse or carrying over to the next pulse.

Ongoing validation of computational models will support model refinement. Our novel ECT simulation pipeline made several predictions supported by existing clinical data: 1) Even under well-controlled electrode preparations conditions, an imperfect correlation between static and dynamic impedance [12] that is explained by current-insensitive scalp impedance (σ_{DS}) while limited by current-dependent scalp conductivity ($\sigma_{\overline{SS}}$); with 2) Limited relative impact of gross anatomy on impedance [6,53]; 3) An imperfect positive correlation between RUL dynamic impedance and motor cortex electric field (Fig. 6 C1), reflected in an inverse relationship between dynamic impedance and seizure threshold [6,9]; 4) an inverse (power law) relationship between moderate decreases in applied ECT voltage/current and dynamic impedance (Fig. 8 [5,11]).

CRediT authorship contribution statement

Gozde Unal: Conceptualization, Software, Analysis, Writing – review & editing. **Jaiti K. Swami:** Conceptualization, Software, Analysis, Writing – review & editing. **Carliza Canela:** Software, Analysis, Writing – review & editing. **Samantha L. Cohen:** Code, Analysis, Writing – review & editing. **Niranjan Khadka:** Analysis, Writing – review & editing. **Mohamad FallahRad:** Code, Analysis, Writing – review & editing. **Baron Short:** Data curation, Writing – review & editing. **Miklos Argyelan:** Data curation, Writing – review & editing. **Harold A. Sackeim:** Conceptualization, Data curation, Writing – review & editing. **Marom Bikson:** Conceptualization, Analysis, Writing – review & editing.

Declaration of competing interest

The City University of New York (CUNY) has IP on neurostimulation systems and methods with authors NK and MB as inventors. MB has equity in Soterix Medical. MB served on the advisory boards, received grants, and/or consulted for Boston Scientific, MECTA Corporation, Halo Neuroscience, Biovisics, and Humm, iLumen, Biovisics, GlaxoSmithKline. HAS serves as a scientific adviser to Cerebral Therapeutics, LivaNova PLC, MECTA Corporation, and Neuronetics Inc. He receives honoraria and royalties from Elsevier, Inc. and Oxford University Press. HAS is the inventor on non-remunerative US patents for Focal Electrically-Administered Seizure Therapy (FEAST), titration in the current domain in ECT, and the adjustment of current in ECT devices, each held by the MECTA Corporation. HAS is also the originator of magnetic seizure therapy (MST).

Acknowledgements

MB is supported by grants from the National Institutes of Health: NIH-NIDA UG3DA048502, NIH-NIGMS T34GM137858 NIH-NINDS 1R01NS112996, NIH-NIMH 1R01NS101362, NIH-NIMH 1R01MH111896, and NIH-NINDS 1R01NS095123.

References

[1] Peterchev AV, Rosa MA, Deng Z-D, Prudic J, Lisanby SH. Electroconvulsive therapy stimulus parameters: rethinking dosage. J ECT 2010;26:159–74. https://doi.org/10.1097/YCT.0b013e3181e48165.
[2] Peterchev AV, Wagner TA, Miranda PC, Nitsche MA, Paulus W, Lisanby SH, et al. Fundamentals of transcranial electric and magnetic stimulation dose: definition, selection, and reporting practices. Brain Stimul 2012;5:435–53. https://doi.org/10.1016/j.brs.2011.10.001.
[3] Sackeim HA, Prudic J, Devanand DP, Nobler MS, Lisanby SH, Peyser S, et al. A prospective, randomized, double-blind comparison of bilateral and right unilateral electroconvulsive therapy at different stimulus intensities. Arch Gen Psychiatr 2000;57:425–34. https://doi.org/10.1001/archpsyc.57.5.425.
[4] Weiner RD, Rogers HJ, Davidson JR, Squire LR. Effects of stimulus parameters on cognitive side effects. Ann N Y Acad Sci 1986;462:315–25. https://doi.org/10.1111/j.1749-6632.1986.tb51266.x.
[5] Umlauf CW, Gunter RC, Tunnicliffe WW. Impedance of the human head as observed during electro-shock treatment. Confin Neurol 1951;11:129–38. https://doi.org/10.1159/000105632.
[6] Delva NJ, Brunet D, Hawken ER, Kesteven RM, Lawson JS, Lywood DW, et al. Electrical dose and seizure threshold: relations to clinical outcome and cognitive effects in bifrontal, bitemporal, and right unilateral ECT. J ECT 2000;16:361–9. https://doi.org/10.1097/00124509-200012000-00006.
[7] Chung KF, Wong SJ. Stimulus dose titration for electroconvulsive therapy. Psychiatr Clin Neurosci 2001;55:105–10. https://doi.org/10.1046/j.1440-1819.2001.00795.x.
[8] Coffey CE, Lucke J, Weiner RD, Krystal AD, Aque M. Seizure threshold in electroconvulsive therapy (ECT) II. The anticonvulsant effect of ECT. Biol Psychiatr 1995;37:777–88. https://doi.org/10.1016/0006-3223(95)00053-J.
[9] van Waarde JA, van Oudheusden LJB, Verwey B, Giltay EJ, van der Mast RC. Clinical predictors of seizure threshold in electroconvulsive therapy: a prospective study. Eur Arch Psychiatr Clin Neurosci 2013;263:167–75. https://doi.org/10.1007/s00406-012-0342-7.
[10] Sackeim HA, Long J, Luber B, Moeller JR, Prohovnik I, Devanand DP, et al. Physical properties and quantification of the ECT stimulus: I. Basic principles. Convuls Ther 1994;10:93–123.
[11] Maxwell RDH. Electrical factors in electroconvulsive therapy. Acta Psychiatr Scand 1968;44:436–48. https://doi.org/10.1111/j.1600-0447.1968.tb07648.x.
[12] Abrams R. Electroconvulsive therapy. fourth ed. Oxford, New York: Oxford University Press; 2002.
[13] Lee WH, Deng Z-D, Kim T-S, Laine AF, Lisanby SH, Peterchev AV. Regional electric field induced by electroconvulsive therapy: a finite element simulation study. In: Conf proc IEEE eng med biol soc, 2010; 2010. p. 2045–8. https://doi.org/10.1109/IEMBS.2010.5626553.
[14] Bai S, Gálvez V, Dokos S, Martin D, Bikson M, Loo C. Computational models of Bitemporal, Bifrontal and Right Unilateral ECT predict differential stimulation of brain regions associated with efficacy and cognitive side effects. Eur Psychiatr 2017;41:21–9. https://doi.org/10.1016/j.eurpsy.2016.09.005.
[15] Lisanby SH. Electroconvulsive therapy for depression. N Engl J Med 2007;357:1939–45. https://doi.org/10.1056/NEJMct075234.
[16] Sackeim HA, Prudic J, Nobler MS, Fitzsimons L, Lisanby SH, Payne N, et al. Effects of pulse width and electrode placement on the efficacy and cognitive effects of electroconvulsive therapy. Brain Stimul 2008;1:71–83. https://doi.org/10.1016/j.brs.2008.03.001.
[17] Argyelan M, Lencz T, Kaliora S, Sarpal DK, Weissman N, Kingsley PB, et al. Subgenual cingulate cortical activity predicts the efficacy of electroconvulsive therapy. Transl Psychiatry 2016;6. https://doi.org/10.1038/tp.2016.54. e789.
[18] Chizmadzhev YA, Indenbom AV, Kuzmin PI, Galichenko SV, Weaver JC, Potts RO. Electrical properties of skin at moderate voltages: contribution of appendageal macropores. Biophys J 1998;74:843–56. https://doi.org/10.1016/S0006-3495(98)74008-1.
[19] Vargas Luna JL, Krenn M, Cortés Ramírez JA, Mayr W. Dynamic impedance model of the skin-electrode interface for transcutaneous electrical stimulation. PloS One 2015;10. https://doi.org/10.1371/journal.pone.0125609. e0125609.
[20] Dorgan SJ, Reilly RB. A model for human skin impedance during surface functional neuromuscular stimulation. IEEE Trans Rehabil Eng 1999;7:341–8. https://doi.org/10.1109/86.788470.
[21] Gomez-Tames J, Sugiyama Y, Laakso I, Tanaka S, Koyama S, Sadato N, et al. Effect of microscopic modeling of skin in electrical and thermal analysis of transcranial direct current stimulation. Phys Med Biol 2016;61:8825–38. https://doi.org/10.1088/1361-6560/61/24/8825.
[22] Yamamoto T, Yamamoto Y. [Electrical properties of the epidermal stratum corneum]. Iyo Denshi Seitai Kogaku 1973;11:337–43.
[23] Jiang J, Truong DQ, Esmaeilpour Z, Huang Y, Badran BW, Bikson M. Enhanced tES and tDCS computational models by meninges emulation. J Neural Eng 2020:17. https://doi.org/10.1088/1741-2552/ab549d. 016027.
[24] Datta A, Bansal V, Diaz J, Patel J, Reato D, Bikson M. Gyri-precise head model of transcranial direct current stimulation: improved spatial focality using a ring

electrode versus conventional rectangular pad. Brain Stimul 2009;2:201–7. 207.e1.
[25] Truong DQ, Magerowski G, Blackburn GL, Bikson M, Alonso-Alonso M. Computational modeling of transcranial direct current stimulation (tDCS) in obesity: impact of head fat and dose guidelines. Neuroimage: Clinic 2013;2:759–66. https://doi.org/10.1016/j.nicl.2013.05.011.
[26] Plonsey R, Heppner DB. Considerations of quasi-stationarity in electrophysiological systems. Bull Math Biophys 1967;29:657–64. https://doi.org/10.1007/bf02476917.
[27] Russell RW, Pierce JF, Townsend JC. Characteristics of tissue impedance in the rat under conditions of electroconvulsive shock stimulation. Am J Physiol 1949;156:317–21. https://doi.org/10.1152/ajplegacy.1949.156.3.317.
[28] Offner F. Electrical properties of tissues in shock therapy. PSEBM (Proc Soc Exp Biol Med) 1942;49:571–5. https://doi.org/10.3181/00379727-49-13633.
[29] Bossetti CA, Birdno MJ, Grill WM. Analysis of the quasi-static approximation for calculating potentials generated by neural stimulation. J Neural Eng 2008;5:44–53.
[30] Ashburner J, Friston KJ. Unified segmentation. Neuroimage 2005;26:839–51. https://doi.org/10.1016/j.neuroimage.2005.02.018.
[31] Huang Y, Dmochowski JP, Su Y, Datta A, Rorden C, Parra LC. Automated MRI segmentation for individualized modeling of current flow in the human head. J Neural Eng 2013:10. https://doi.org/10.1088/1741-2560/10/6/066004. 066004.
[32] Kibret B, Premaratne M, Sullivan C, Thomson RH, Fitzgerald PB. Electroconvulsive therapy (ECT) during pregnancy: quantifying and assessing the electric field strength inside the foetal brain. Sci Rep 2018;4128:8. https://doi.org/10.1038/s41598-018-22528-x.
[33] Bikson M, Dmochowski J, Rahman A. The "quasi-uniform" assumption in animal and computational models of non-invasive electrical stimulation. Brain Stimul 2013;6:704–5. https://doi.org/10.1016/j.brs.2012.11.005.
[34] Bikson M, Truong DQ, Mourdoukoutas AP, Aboseria M, Khadka N, Adair D, et al. Modeling sequence and quasi-uniform assumption in computational neurostimulation. Prog Brain Res 2015;222:1–23. https://doi.org/10.1016/bs.pbr.2015.08.005.
[35] Steward B, Bakir AA, Martin D, Dokos S, Loo CK. The left anterior right temporal (LART) placement for electroconvulsive therapy: a computational modelling study. Psychiatry Res Neuroimaging 2020:304. https://doi.org/10.1016/j.pscychresns.2020.111157. 111157.
[36] Lee WH, Lisanby SH, Laine AF, Peterchev AV. Minimum electric field exposure for seizure induction with electroconvulsive therapy and magnetic seizure therapy. Neuropsychopharmacology 2017;42:1192–200. https://doi.org/10.1038/npp.2016.276.
[37] Lee WH, Lisanby SH, Laine AF, Peterchev AV. Electric field characteristics of electroconvulsive therapy with individualized current amplitude: a preclinical study. Conf.Proc.IEEE.Eng.Med.Biol.Soc 2013;2013:3082–5. https://doi.org/10.1109/EMBC.2013.6610192.
[38] Bai S, Loo C, Dokos S. Effects of electroconvulsive therapy stimulus pulsewidth and amplitude computed with an anatomically-realistic head model. Annu Int Conf IEEE Eng Med Biol Soc 2012;2012:2559–62. https://doi.org/10.1109/EMBC.2012.6346486.
[39] McCall WV. In: Charles H Kellner, editor. Handbook of ECT: a guide to electroconvulsive therapy for practitioners, 35. New York: Cambridge University Press; 2019. p. 144. https://doi.org/10.1097/YCT.0000000000000591. ISBN 978-1-108-40328-3. The Journal of ECT 2019.
[40] Datta A, Truong D, Minhas P, Parra LC, Bikson M. Inter-individual variation during transcranial direct current stimulation and normalization of dose using MRI-derived computational models. Front Psychiatr 2012;91:3. https://doi.org/10.3389/fpsyt.2012.00091.
[41] Edwards D, Cortes M, Datta A, Minhas P, Wassermann EM, Bikson M. Physiological and modeling evidence for focal transcranial electrical brain stimulation in humans: a basis for high-definition tDCS. Neuroimage 2013;74:266–75. https://doi.org/10.1016/j.neuroimage.2013.01.042.
[42] Huang Y, Liu AA, Lafon B, Friedman D, Dayan M, Wang X, et al. Measurements and models of electric fields in the in vivo human brain during transcranial electric stimulation. Elife 2017:6. https://doi.org/10.7554/eLife.18834.
[43] Argyelan M, Oltedal L, Deng Z-D, Wade B, Bikson M, Joanlanne A, et al. Electric field causes volumetric changes in the human brain. Elife 2019;8. https://doi.org/10.7554/eLife.49115.
[44] Datta A, Bikson M, Fregni F. Transcranial direct current stimulation in patients with skull defects and skull plates: high-resolution computational FEM study of factors altering cortical current flow. Neuroimage 2010;52:1268–78.
[45] Truong DQ, Magerowski G, Pascual-Leone A, Alonso-Alonso M, Bikson M. Finite Element study of skin and fat delineation in an obese subject for transcranial Direct Current Stimulation. In: 2012 annual international conference of the IEEE engineering in medicine and biology society (EMBC); 2012. p. 6587–90. https://doi.org/10.1109/EMBC.2012.6347504.
[46] Railton R, Fisher J, Sinclair A, Shrigmankar JM. Comparison of electrical measurements on constant voltage and constant current ECT machines. Br J Psychiatry 1987;151:244–7. https://doi.org/10.1192/bjp.151.2.244.
[47] Dmochowski JP, Datta A, Bikson M, Su Y, Parra LC. Optimized multi-electrode stimulation increases focality and intensity at target. J Neural Eng 2011:8. https://doi.org/10.1088/1741-2560/8/4/046011. 046011.
[48] Khadka N, Bikson M. Role of skin tissue layers and ultra-structure in transcutaneous electrical stimulation including tDCS. Phys Med Biol 2020. https://doi.org/10.1088/1361-6560/abb7c1.
[49] Panescu D, Webster JG, Stratbucker RA. A nonlinear finite element model of the electrode-electrolyte-skin system. IEEE Trans Biomed Eng 1994;41:681–7. https://doi.org/10.1109/10.301735.
[50] Sha N, Kenney LPJ, Heller BW, Barker AT, Howard D, Moatamedi M. A finite element model to identify electrode influence on current distribution in the skin. Artif Organs 2008;32:639–43. https://doi.org/10.1111/j.1525-1594.2008.00615.x.
[51] Wake K, Sasaki K, Watanabe S. Conductivities of epidermis, dermis, and subcutaneous tissue at intermediate frequencies. Phys Med Biol 2016;61:4376–89. https://doi.org/10.1088/0031-9155/61/12/4376.
[52] Yamamoto T, Yamamoto Y. Analysis for the change of skin impedance. Med Biol Eng Comput 1977;15:219–27. https://doi.org/10.1007/BF02441041.
[53] Sackeim H, Decina P, Prohovnik I, Malitz S. Seizure threshold in electroconvulsive therapy. Effects of sex, age, electrode placement, and number of treatments. Arch Gen Psychiatr 1987;44:355–60. https://doi.org/10.1001/archpsyc.1987.01800160067009.
[54] Peterchev AV, Krystal AD, Rosa MA, Lisanby SH. Individualized low-amplitude seizure therapy: minimizing current for electroconvulsive therapy and magnetic seizure therapy. Neuropsychopharmacology 2015;40:2076–84. https://doi.org/10.1038/npp.2015.122.
[55] Loo CK, Bai S, Martin D, Gálvez V, Dokos S. Revisiting frontoparietal montage in electroconvulsive therapy: clinical observations and computer modeling: a future treatment option for unilateral electroconvulsive therapy. J ECT 2015;31:e7–13. https://doi.org/10.1097/YCT.0000000000000147.
[56] Rosa MA, Abdo GL, Lisanby SH, Peterchev A. Seizure induction with low-amplitude-current (0.5 A) electroconvulsive therapy. J ECT 2011;27:341–2. https://doi.org/10.1097/YCT.0b013e31822149db.
[57] Nadeem M, Thorlin T, Gandhi OP, Persson M. Computation of electric and magnetic stimulation in human head using the 3-D impedance method. IEEE (Inst Electr Electron Eng) Trans Biomed Eng 2003;50:900–7.
[58] Szmurlo R, Sawicki B, Starzynski J, Wincenciak S. A comparison of two models of electrodes for ECT simulations. IEEE Trans Magn 2006;42:1395–8. https://doi.org/10.1109/TMAG.2006.871580.
[59] Merrill DR, Bikson M, Jefferys JG. Electrical stimulation of excitable tissue: design of efficacious and safe protocols. J Neurosci Methods 2005;141:171–98.
[60] Shahid SS, Bikson M, Salman H, Wen P, Ahfock T. The value and cost of complexity in predictive modelling: role of tissue anisotropic conductivity and fibre tracts in neuromodulation. J Neural Eng 2014:11. https://doi.org/10.1088/1741-2560/11/3/036002. 036002.